Journal of Solid State Chemistry 182 (2009) 187–195

Contents lists available at ScienceDirect

Journal of Solid State Chemistry

journal homepage: www.elsevier.com/locate/jssc

Synthesis and structural characterization of $La_xSr_{1-x}MnO_{2.6+\delta}$ $(0.1<x<0.4)$ compounds displaying compressed octahedral coordination of $Mn^{(4-5x)+}$ ☆

Leopoldo Suescun [a,c,*], Bogdan Dabrowski [b,c], Steven Remsen [b], James Mais [b]

[a] Cryssmat-Lab/Cátedra de Física/Detema, Facultad de Química, Universidad de la República, P.O. Box 1157, Montevideo, Uruguay
[b] Physics Department, Northern Illinois University, DeKalb, IL 60115, USA
[c] Materials Science Division, Argonne National Laboratory, Argonne, IL 60439, USA

ARTICLE INFO

Article history:
Received 1 August 2008
Received in revised form
14 October 2008
Accepted 18 October 2008
Available online 29 October 2008

Keywords:
Manganites
Oxygen-vacancy-ordering
Electronic configuration
LaMnO3
Phase transition

ABSTRACT

$La_xSr_{1-x}MnO_{2.6+\delta}$ $(x=0.1–0.4)$ compounds have been obtained by low-temperature annealing of stoichiometric materials in hydrogen. $La_{0.1}Sr_{0.9}MnO_{2.6+\delta}$ $(\delta=0.15)$ and $La_{0.3}Sr_{0.7}MnO_{2.6}$, tetragonal $(P4/m)$, and $La_{0.2}Sr_{0.8}MnO_{2.6}$, pseudo-tetragonal monoclinic $(P2/m)$, structures are isostructural with oxygen-vacancy-ordered $Sr_5Mn_5O_{13}$ $(a=b\approx\sqrt{5}a_P,\ c\approx a_P)$. $La_{0.4}Sr_{0.6}MnO_{2.6}$ shows cubic perovskite structure with disordered oxygen vacancies. In the vacancy-ordered $(La_xSr_{1-x})_5Mn_5O_{13}$ phases four out of five Mn cations are Mn^{3+} and show a typical Jahn-Teller elongated pyramidal coordination while the fifth one $Mn^{(4-5x)+}$, in octahedral environment, shows decreasing formal charge from Mn^{4+} $(x=0)$ to $Mn^{2.5+}$ $x=0.3$. This unusual selective doping of the octahedral site produces structural strain due to increasing size of the $Mn^{(4-5x)+}$ and, in the case of $(La_{0.2}Sr_{0.8})_5Mn_5O_{13}$, the unusual compressed octahedral arrangement of oxygen atoms around it. The coordination geometry implies that either the $d_{x^2-y^2}$ orbital is occupied, which would be a rare example of inverted occupancy of e_g orbitals in manganites, or that disordered Mn^{3+} apically elongated MnO_6 octahedra are present with normal electronic configuration $d^3_{t_{2g}}d^0_{x^2-y^2}d^1_{z^2}$, and the observed bond distances are the average of the long and intermediate in-plane Mn–O bonds. Several structural features favor the second case.

1. Introduction

Oxygen-vacancy ordering in perovskites has been a topic of intense research for decades [1]. Vacancy ordering phenomena have been important to understanding conducting, magnetic and superconducting properties of technologically important materials such as solid oxide fuel cell (SOFC) cathodes and high-temperature superconducting cuprates. The large amount of information accumulated for Cu-containing perovskites, although serving as a guide for the possible orderings, could not be directly applied to other 3d transition metal elements due to the differences in the electronic structures and cation sizes that determine the bonding and coordination preferences. Recently, we have been studying mixed electronic and ionic conductivity in the lightly La-substituted $La_xSr_{1-x}MnO_y$ system, which exhibits complex vacancy-ordered phases [2–4]. The formation of these phases poses a difficulty for the development of practical devices due to deleterious decreases of electrical and ionic conductivity resulting from charge ordering. Knowledge of the structure and stability of vacancy-ordered phases is of critical importance for future advances in SOFC cathodes [5]. Several phases have been described for the $La_xSr_{1-x}MnO_y$ system with vacancy ordering arrangements dictated by the coordination preferences and the ratios of the Mn^{2+}, Mn^{3+} and Mn^{4+} ions [2–8]. Among them, the brownmillerite-type structure [9] observed in $La_xSr_{1-x}MnO_{2.5}$ $(x=0.6,\ 0.75$ and $0.8)$ [8] contains tetrahedral Mn^{2+} and octahedral Mn^{2+}/Mn^{3+} coordinated cations that differ from the $Ca_2Mn_2O_5$ structure type [10] observed in $La_xSr_{1-x}MnO_{2.5}$ for $x=0$ and 0.1 [2–4] where only pyramids of Mn^{3+} or Mn^{2+}/Mn^{3+} are observed. At higher oxygen contents, structures closely related to the brownmillerite have been described for the La-rich compositions $La_8Mn_8O_{23}$ $(LaMnO_{2.875})$ and $La_4Mn_4O_{11}$ $(LaMnO_{2.75})$ [7]. For the Sr-rich compositions the following structures related to $Ca_2Mn_2O_5$ have been observed: $Sr_5Mn_5O_{13}$ $(SrMnO_{2.6})$, $Sr_7Mn_7O_{19}$ $(SrMnO_{2.714})$ [3], $(La_{0.1}Sr_{0.9})_2Mn_2O_{5.1}$ $(La_{0.1}Sr_{0.9}MnO_{2.55})$, $(La_{0.2}Sr_{0.8})_5Mn_5O_{13}$ $(La_{0.2}Sr_{0.8}MnO_{2.6})$ and $(La_{0.3}Sr_{0.7})_5Mn_5O_{13.25}$

☆ Further details of the crystal structure investigations may be obtained from Fachinformationszentrum Karlsruhe, 76344 Eggenstein-Leopoldshafen, Germany (fax: (+49)7247-808-666; e-mail: crysdata@fiz-karlsruhe.de, http://www.fiz-karlsruhe.de/ecid/Internet/en/DB/icsd/depot_anforderung.html) on quoting the deposition numbers CSD-419750 for $(La_{0.1}Sr_{0.9})_5Mn_5O_{13.77}$, CSD-419751 for $(La_{0.2}Sr_{0.8})_5Mn_5O_{13}$, CSD-419752 for $(La_{0.3}Sr_{0.7})_5Mn_5O_{13}$ and CSD-417653 for $La_{0.4}Sr_{0.6}MnO_{2.6}$.

* Corresponding author at: Cryssmat-Lab/Cátedra de Física/Detema, Facultad de Química, Universidad de la República, P.O. Box 1157, Montevideo, Uruguay. Fax: +598 2 9241906.
E-mail address: leopoldo@fq.edu.uy (L. Suescun).

0022-4596/$ - see front matter © 2008 Elsevier Inc. All rights reserved.
doi:10.1016/j.jssc.2008.10.020

($La_{0.3}Sr_{0.7}MnO_{2.65}$) [2]. In particular, oxygen-vacancy-ordered $SrMnO_y$ ($y = 2.5$, 2.6 and 2.714) were found to form the $Sr_{4+n}Mn_4^{3+}Mn^{4+}{}_nO_{10+3n}$ homologous series of compounds [3,11] exhibiting very interesting orbital ordering features as a result of the charge separation of Mn^{3+} and Mn^{4+} in pyramids and octahedra, respectively.

We have been systematically studying the structure and properties of oxygen-vacancy-ordered arrangements for $La_xSr_{1-x}MnO_y$ compounds in the range $0 \leqslant x \leqslant 0.5$ and $2.5 \leqslant y \leqslant 3$. Neutron powder diffraction was used as the structural characterization technique as it provides accurate atomic coordinates and allows precise determination of the subtle structural distortions associated with the vacancy ordering. In this paper we describe the preparation and structures of the $La_xSr_{1-x}MnO_{2.6}$ ($0.1 \leqslant x \leqslant 0.4$) compounds closely related to the $Sr_5Mn_4^{3+}Mn^{4+}O_{13}$ ($SrMnO_{2.6}$), displaying apparent compressed octahedral coordination geometry around $Mn^{(4-5x)+}$ and a compositional order-disorder phase transition as a function of La substitution.

2. Experimental

Sample preparation and thermogravimetric analysis: Synthesis of the $La_xSr_{1-x}MnO_y$ ($y = 2.6$, $x = 0.1$–0.4) samples was achieved by using three-step solid state reaction of appropriate amounts of MnO_2, La_2O_3 and $SrCO_3$ (all >99.99% purity). The oxygen-deficient perovskites were prepared in the first step using low partial pressure of oxygen at ~1400 °C since the synthesis of the Sr-rich compositions in air is complicated by the relatively small size of Mn^{4+} cation with respect to Sr^{2+} and La^{3+} which results in formation of hexagonal 4 layer phase [12]. In the second step, the oxygen-deficient materials were annealed in air between 400 and 500 °C to achieve stoichiometric oxygen content. This procedure has been previously applied for preparation of $La_xSr_{1-x}MnO_3$ materials ($0 < x < 0.5$) [13] and was used in this work to obtain starting materials for the preparation of oxygen-deficient phases. The annealing conditions for preparation of vacancy-ordered compounds were established from thermogravimetric measurements (Cahn TG171). Fig. 1 shows the reduction of stoichiometric $La_xSr_{1-x}MnO_3$ samples ($x = 0.1$–0.4) using 48% H_2 in Ar gas flow (60 sccm) with very slow heating rate of 0.1°/min. The samples, consisting of a crushed pellet of material with initial weights between 0.85 ($x = 0.4$) and 0.90 ($x = 0.1$) g, show weight loss starting at ~200 °C which proceeds monotonically until decomposition above 600 °C. The curves show slope changes that could be associated with the formation of stable phases displaying particular oxygen contents at certain temperatures. The most significant slope changes observed near $y \approx 2.6$ at 350–450 °C are associated with a stable equilibrium of the $O_{2.6}$ phases for samples with $x = 0.2$, 0.3 and 0.4. The $La_{0.1}Sr_{0.9}MnO_y$ ($x = 0.1$) sample differs from others through a less visible slope change that occurs over a broad range of oxygen contents with a slightly more pronounced change at $y \approx 2.55$ corresponding to an average Mn^{3+} content and vacancy-ordered $La_{0.1}Sr_{0.9}MnO_{2.55}$ phase, in accord

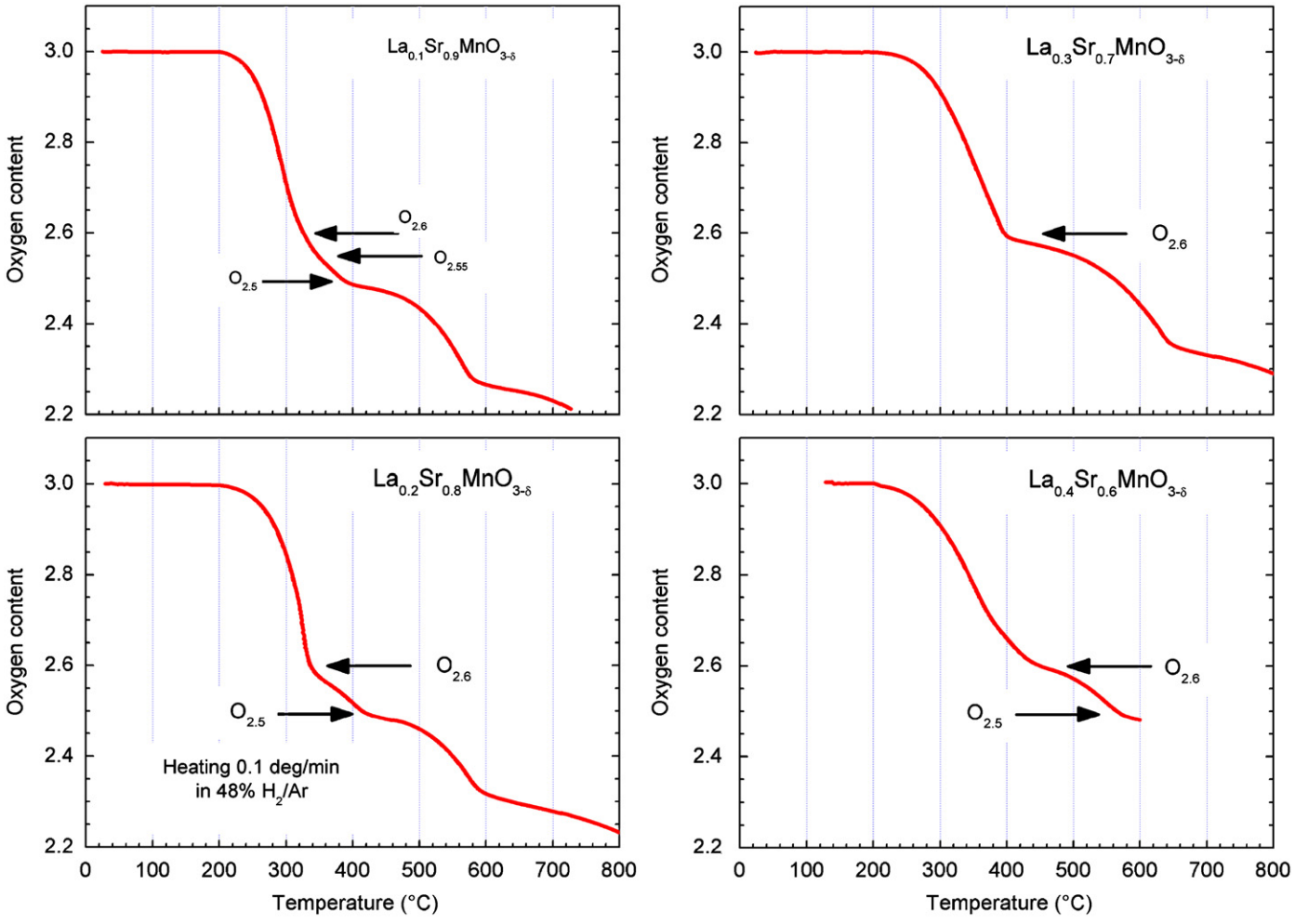

Fig. 1. Reduction of $La_xSr_{1-x}MnO_3$, $x = 0.1$ (left) to $x = 0.4$ (right) samples in 48% H_2/Ar flow (60 sccm) with 0.1°/min heating rate.

with previous observations [2,4]. Based on the TGA data the $La_xSr_{1-x}MnO_{2.6}$ samples with $x \neq 0.1$ were prepared in the third step of synthesis as follow. Approximately 1.5 g of oxygen stoichiometric samples with $x = 0.2$, 0.3 and 0.4 were annealed in flowing H_2 in a tube furnace at 300, 360 and 365 °C, respectively, during two 20 h annealing periods. The oxygen content of these samples was determined with a precision of 0.01 atoms per formula unit from the mass change observed after re-oxidation of ~250 mg of the reduced material in air at 500 °C for 12 h that yielded the stoichiometric $La_xSr_{1-x}MnO_3$ compounds. The oxygen contents of reduced compounds was found $y = 2.59(1)$, 2.61(1) and 2.62(1) for $x = 0.2$, 0.3 and 0.4, respectively. The absence of a plateau at $y = 2.6$ for $x = 0.1$ prevented us from preparation of a stoichiometric sample $La_{0.1}Sr_{0.9}MnO_{2.6}$. The sample obtained from firing $La_{0.1}Sr_{0.9}MnO_3$ in Ar at 1350 °C with an oxygen content $y = 2.74(1)$ showed similar structural arrangement to $x = 0.2$ and 0.3 samples, therefore it was used for the structural characterization of the series. The phase purity of all samples after every synthesis step was checked by conventional X-ray powder diffraction using a Rigaku D-MAX diffractometer.

Topotactic reduction at low temperatures usually leads to samples characterized by presence of structural inhomogeneities and small crystalline domains. X-ray data for $x = 0.2$ and 0.3 samples showed significant broadening of superstructure peaks originating from the oxygen-vacancy ordering. This suggested presence of small coherently scattering domains of the anion sublattice within the grains (note that the cation sub-lattice is almost unchanged with respect to the cubic perovskite precursor apart from small shifts around vacant sites). Since previous results showed that $La_{0.2}Sr_{0.8}MnO_{2.6}$ with fixed oxygen content undergoes a reversible vacancy order-disorder transition at ~700 °C [4] we have attempted to improve the crystallinity of the samples by annealing. A portion of the $La_{0.2}Sr_{0.8}MnO_{2.59}$ sample (#1) was annealed in pure Ar (~0.1 ppm O_2) at 800 °C for 2 h and slowly cooled to 500 °C, to give sample (#2), to allow oxygen-vacancy reordering into larger domains. Another attempt was made to prepare a $La_{0.2}Sr_{0.8}MnO_{2.6}$ sample away from the equilibrium conditions by a controlled reduction of $La_{0.2}Sr_{0.8}MnO_3$ in 1%H_2/Ar at 1300 °C to $y = 2.6$ on the thermobalance, followed by slow cooling to room temperature in pure Ar to give sample (#3). Although this last sample showed slightly narrower peaks, none of these attempts improve crystallinity significantly, indicating that the small coherent oxygen-vacancy-ordered regions appear to be intrinsic to the structure in accord with structural features that will be discussed in the following paragraphs.

Neutron powder diffraction data collection and analysis: Samples of $La_xSr_{1-x}MnO_{2.6}$ with $x = 0.1$, 0.2 (#1, #2 and #3), 0.3 and 0.4 were analyzed by neutron time-of-flight powder diffraction at Argonne's Intense Pulsed Neutron Source (SEPD (Special Environment Powder Diffractometer)) and (GPPD (General Purpose Powder Diffractometer)) stations [14]. Different instruments were used to obtain high-intensity high-resolution (GPPD) or high d-spacing range (SEPD) data to perform the structural characterization of the samples. The data was analyzed by the Rietveld Method using the GSAS/EXPGUI [15,16] suite of programs. High-resolution GPPD data was collected for the $x = 0.2$ (#1 and #3), the $x = 0.3$ and $x = 0.4$ samples in order to provide better description of the monoclinic distortion of $La_{0.2}Sr_{0.8}MnO_{2.6}$, rule out the presence of a similar distortion in $La_{0.3}Sr_{0.7}MnO_{2.6}$, and rule-out distortions from cubic symmetry in $La_{0.4}Sr_{0.6}MnO_{2.6}$. High d-spacing SEPD data was collected for the $x = 0.1$ (previously identified as tetragonal [4]) and $x = 0.2$ (#2) samples. Two data banks (1 and 5 for GPPD data and 1 and 3 for SEPD data) were simultaneously fit to access the highest d-spacing reflections available ($d_{max} = 4.5$ and 9 Å for GPPD Bank 5 and SEPD Bank 3, respectively). Background, absorption, and geometrical corrections were refined for each data bank. The broadening of superstructure peaks observed for $x = 0.1$, 0.2 and 0.3 samples was successfully modeled using the Stephens formulation [17] implemented in profile function 4 in GSAS. In all cases, the symmetry-allowed coordinates and independent isotropic displacement parameters were refined for each La/Sr and O site and one global thermal parameter was refined for all Mn atoms to avoid unphysical values. Anisotropic displacement parameters were refined for O atoms in $La_{0.1}Sr_{0.9}MnO_{2.6+\delta}$, $La_{0.3}Sr_{0.7}MnO_{2.6}$ and $La_{0.4}Sr_{0.6}MnO_{2.6}$ but not in $La_{0.2}Sr_{0.8}MnO_{2.6}$ where correlations of parameters in the pseudo-tetragonal cell lead to non-positive definite ellipsoids. Site occupation factor (S.O.F.) of partially occupied oxygen vacant sites was refined for $La_{0.1}Sr_{0.9}MnO_{2.6+\delta}$ where significant occupation was expected and for $La_{0.4}Sr_{0.6}MnO_{2.6}$ where the structure was cubic. For the rest of the compositions the oxygen contents were fixed at 2.6, in accordance with TGA data. La/Sr occupation was refined on various sites but no clear indication of ordering was obtained, therefore, a fully disordered model was adopted for all the structures. Initial refinements of oxygen's anisotropic displacement parameter in the vacancy-disordered $La_{0.4}Sr_{0.6}MnO_{2.6}$ cubic phase (space group Pm3m) showed a huge anisotropy between the directions along and perpendicular to the Mn–O bond. This suggested that the O1 atom was displaced from the 3d Wyckoff site (0.5, 0, 0) in the plane normal to the Mn–O bond. The atom was placed at 12 h site (0.5, ε, 0), allowing ε, the S.O.F and the anisotropic displacement parameters to refine. The refined value of ε converged to 0.061(4) corresponding to a shift of 0.24(1) Å from the ideal position. This significant deviation of the O atom from its ideal position is an indication of the possible short-range ordering of vacancies that do not extend far enough in the crystallites to produce long-range order necessary for the observation of a non-cubic diffraction pattern. Fig. 2(a–d) shows the fitted patterns and Table 1 lists final refined parameters and residuals. In the case of $x = 0.2$ $La_{0.2}Sr_{0.8}MnO_{2.6}$, the results for the sample (#3), obtained from reduction at 1300 °C (1% H_2/Ar) and slow cooling in Ar on TGA, are presented. Details of fitted patterns demonstrating splitting of cubic 221/300 and 220 peaks are shown in Fig. 3(a–d). The larger degree of structural distortion observed for monoclinic P2/m $La_{0.2}Sr_{0.8}MnO_{2.6}$ sample is clearly visible in Fig. 3(b). Additionally the existence of local ordering in $x = 0.3$ sample is also visible in Fig. 3(d) in a subtle background increase around $d = 1.29$ Å among other features described above. Fig. 4 shows the final structural models for $La_{0.2}Sr_{0.8}MnO_{2.6}$ (very similar to $x = 0.1$ and 0.3 compounds) and $La_{0.4}Sr_{0.6}MnO_{2.6}$ compounds, and Table 2 lists selected bond distances for the four compounds.

3. Discussion

The stabilization of vacancy-ordered perovskite phases $ABO_{2.6}$ ($ABO_{3-\delta}$ with $\delta = 0.4$ or $A_5B_5O_{13}$) was initially shown for the cuprates $BaLa_4Cu_5O_{13+\delta}$ [18], $La_5Cu_5O_{13+\delta}$ [19], $Nd_5Cu_5O_{13+\delta}$ [20] and recently for manganites $Sr_5Mn_5O_{13}$ [3] and $(La_{0.2}Sr_{0.8})_5Mn_5O_{13}$ [2,4]. In $BaLa_4Cu_5O_{13+\delta}$, the Ba and La are ordered on different crystallographic sites; no such ordering was observed for other compounds. The oxygen-vacancy-ordered compounds $La_xSr_{1-x}MnO_{2.6}$ (or $(La_xSr_{1-x})_5Mn_5O_{13}$) with $x = 0.1$–0.3 show the same vacancy ordering arrangement (see Fig. 4) that produces four square-base pyramidal and one octahedral Mn cations per unit cell. $BaLa_4Cu_5O_{13}$ and $Sr_5Mn_5O_{13}$ display tetragonal symmetry, space group $P4/m$, with $a \approx \sqrt{5}a_P$ and $c \approx a_P$ also observed for $(La_{0.1}Sr_{0.9})_5Mn_5O_{13+\delta}$ and $(La_{0.3}Sr_{0.7})_5Mn_5O_{13+\delta}$. The compounds $La_5Cu_5O_{13+\delta}$ and $Nd_5Cu_5O_{13+\delta}$ have monoclinic symmetry, space group $P2/m$, with pseudo-tetragonal axes $a \approx b \approx \sqrt{5}a_P$, $c \approx a_P$ and

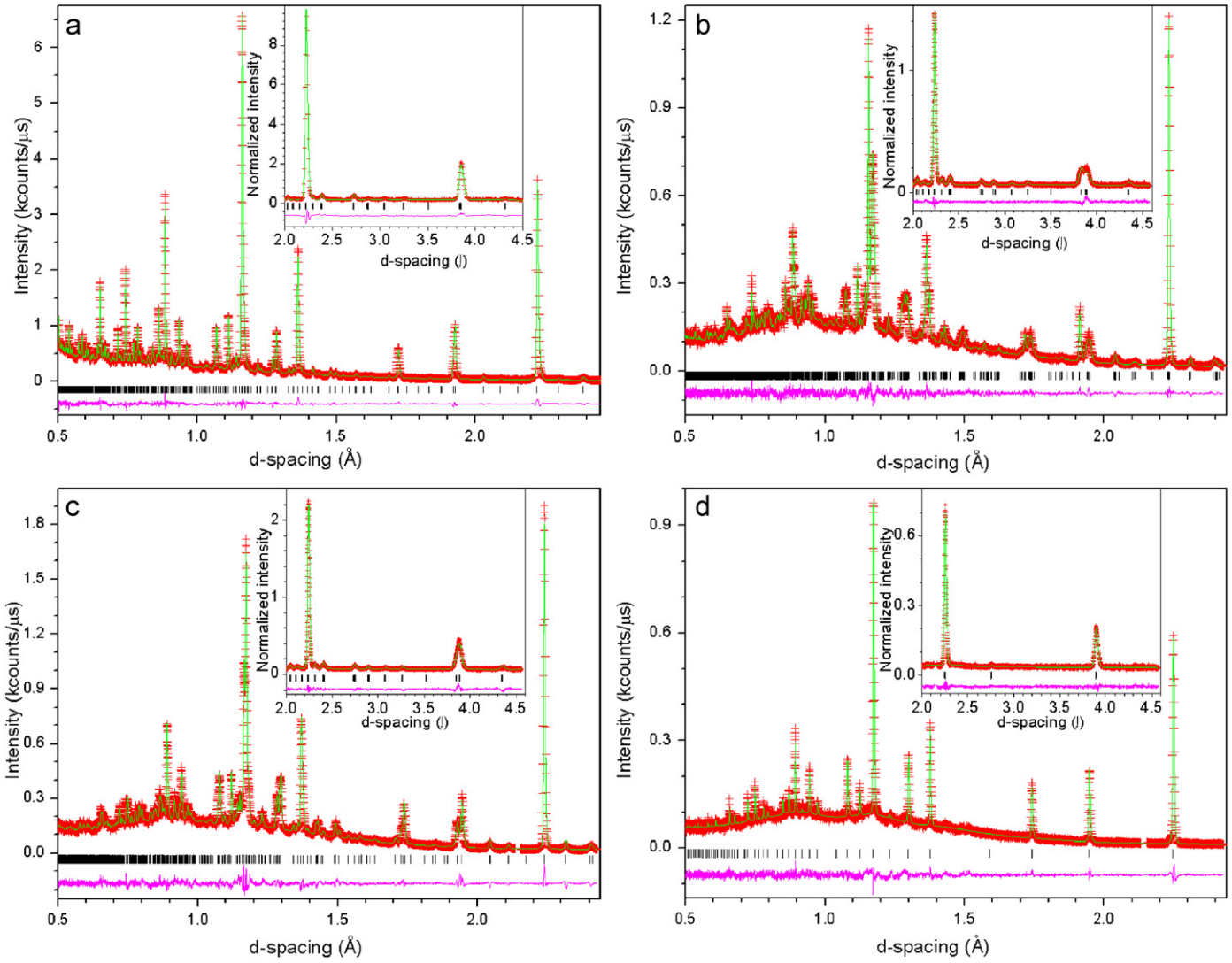

Fig. 2. Rietveld fit of neutron diffraction data for (a) tetragonal $P4/m$ $(La_{0.1}Sr_{0.9})_5Mn_5O_{13.75}$, (b) monoclinic $P2/m$ $(La_{0.2}Sr_{0.8})_5Mn_5O_{13}$, (c) tetragonal $P4/m$ $(La_{0.3}Sr_{0.7})_5Mn_5O_{13}$ and (d) cubic $Pm3m$ $La_{0.4}Sr_{0.6}MnO_{2.6}$. Observed intensities and peak positions are marked with +and | symbols, respectively. The curve through the experimental points is the fit while the curve in the bottom is the difference between observed and calculated intensities. Insets show high d-spacing data normalized by the incident neutron spectrum to enhance the visibility of small superstructure peaks.

$\gamma \approx 90^\circ$ observed in $(La_{0.2}Sr_{0.8})_5Mn_5O_{13}$ [2] (confirmed in this work, as shown in Table 1).

Although the vacancy ordering arrangement is the same for the three ($x = 0.1$, 0.2 and 0.3) compounds, and also similar to $Sr_5Mn_5O_{13}$ ($x = 0$, shown in the first column of Table 2), the reduction of average Mn charge and concomitant increase of the ionic size of Mn with increasing x have significant effect on structural features that will be described in the following discussion.

The $Sr_5Mn_5O_{13}$ compound ($x = 0$) shows charge separation of Mn^{3+} cations in pyramids and Mn^{4+} cations in octahedra (as can be seen in Fig. 4). Additionally, electronic orbital ordering is present for Mn^{3+} where half-occupied d_{z^2} orbitals are aligned along the apical direction of the pyramids showing characteristic bond distances and angles pattern which are also observed in $Sr_2Mn_2O_5$ [3,21] and $Ca_2Mn_2O_5$ manganites [10] and in cuprates [18–20]. This orbital ordering is present for all vacancy-ordered compounds ($x \neq 0.4$), even for $La_{0.1}Sr_{0.9}MnO_{2.6+\delta}$, containing significant amounts of oxygen in the nominally vacant sites. The characteristic separation of pyramidal Mn–O bond lengths into three groups is observed: elongated apical, intermediate equatorial and short equatorial Mn–O bonds with average values of 2.02, 1.93 and 1.86 Å, respectively, similar to observed in $Sr_2Mn_2O_5$ and $Sr_5Mn_5O_{13}$. The long and short Mn–O bonds for two adjacent pyramids correspond to the O atoms that connect their apical and equatorial positions, respectively. This Mn–O bond pattern indicates that the half-occupied d_{z^2} orbital points towards the apical direction of the pyramids and the $d_{x^2-y^2}$ orbital remains empty for the d^4 Mn^{3+} cation that shows the electronic configuration $d^3_{t_{2g}}d^1_{z^2}$. Fig. 5 shows in detail the coordination polyhedra around Mn1 and Mn2/3 sites for $x = 0.2$ compound.

The average charge $4-x-2y$ of Mn in these compounds as a function of x and y is shown in the last row of Table 2. As x increases from 0 to 0.4 the average charge decreases from 3.2+ to 2.8+. However, the constancy of the dimensions of Mn^{3+} pyramids indicates that the extra electrons provided by the La doping are not evenly distributed over both Mn sites, but are added only to the octahedral Mn sites. A similar observation is made for the $x = 0.1$ sample for which excess oxygen seems to dope charge only to the octahedral Mn sites. Considering that four out of five Mn ions in the structure are pyramidal coordinated and remain 3+, the charge of the octahedral Mn^{n+} is changing with substitution x

Table 1
Structural parameters for $La_xSr_{1-x}MnO_{2.6+\delta}$ samples..

		$x = 0.1$	$x = 0.2$	$x = 0.3$	$x = 0.4$
Oxygen Content (y)	Reoxidation	2.74(1)	2.59(1)	2.61(1)	2.62(1)
	Refinement[a]	2.749(2)	2.6	2.6	2.601(6)
	Space Group	P4/m (#83)	P2/m (#10)	P4/m (#83)	Pm3m (#221)
	a (Å)	8.6123(1)	8.6983(1)	8.6921(1)	3.8917(5)
	b (Å)		8.6736(1)		
	c (Å)	3.84084(4)	3.82324(3)	3.85213(7)	
	γ (°)		90.267(3)		
	V (Å^3)	284.8814)	288.444(6)	291.041(6)	58.94(1)
La/Sr1	Wyckoff	1d	1h	1d	1b
	U_{iso} ($\times 100$ Å^2)	0.99(5)	0.71(5)	0.74(12)	2.22(7)
La/Sr2	Wyckoff	4k	2n	4k	
	x	0.1121(2)	0.1164(4)	0.1137(3)	
	Y	0.7128(2)	0.7184(3)	0.7193(3)	
	U_{iso}($\times 100$ Å^2)	0.68(1)	0.10(2)	1.17(6)	
La/Sr3	Wyckoff		2n		
	x		0.2822(3)		
	y		0.1165(4)		
	U_{iso}($\times 100$ Å^2)		0.87(4)		
Mn1	Wyckoff	1a	1a	1a	1a
	U_{iso}[a]($\times 100$ Å^2)	0.59(2)	0.33(3)	0.85(5)	1.28(6)
Mn2	Wyckoff	4j	2m	4j	
	x	0.1986(4)	0.1993(7)	0.2001(5)	
	y	0.4024(4)	0.4020(7)	0.4100(6)	
Mn3	Wyckoff		2m		
	x		0.5879(7)		
	y		0.1958(7)		
O1	Wyckoff	1b	1b	1b	12h[b]
	x				0.061(4)
	$U_{11/iso}$($\times 100$ Å^2)	1.79(6)	1.21(8)	2.83(25)	1.34(12)
	U_{22}($\times 100$ Å^2)	2.22(6)		2.93(29)	5.6(8)
	U_{33}($\times 100$ Å^2)	0.70(5)		1.07(15)	2.8(4)
	U_{12}($\times 100$ Å^2)	−1.75(7)		−1.21(20)	
	S.O.F.				0.2167
O2	Wyckoff	4k	2n	4k	
	x	0.1806(2)	0.1641(4)	0.1766(4)	
	y	0.4074(4)	0.4157(5)	0.4157(6)	
	$U_{11/iso}$($\times 100$ Å^2)	0.94(6)	1.09(6)	1.15(22)	
	U_{22}($\times 100$ Å^2)	3.23(6)		4.52(24)	
	U_{33}($\times 100$ Å^2)	1.65(6)		4.53(23)	
	U_{12}($\times 100$ Å^2)	0.82(9)		2.22(20)	
O3	Wyckoff	4j	2n	4j	
	x	0.0813(2)	0.5814(5)	0.0802(4)	
	y	0.2100(3)	0.1745(4)	0.2226(4)	
	$U_{11/iso}$($\times 100$ Å^2)	3.69(9)	1.05(6)	4.30(26)	
	U_{22}($\times 100$ Å^2)	1.07(6)		3.39(23)	
	U_{33}($\times 100$ Å^2)	0.76(5)		0.54(16)	
	U_{12}($\times 100$ Å^2)	−1.19(8)		−0.90(18)	
O4	Wyckoff	4j	2m	4j	
	x	0.4003(3)	0.0769(4)	0.4010(5)	
	y	0.2904(3)	0.2192(5)	0.3010(7)	
	$U_{11/iso}$($\times 100$ Å^2)	1.73(10)	1.06(6)	3.9(4)	
	U_{33}($\times 100$ Å^2)	0.60(15)		1.0(5)	
O5	Wyckoff		2m		
	x		0.2269(4)		
	y		0.9262(4)		
	U_{iso}($\times 100$ Å^2)		0.80(5)		

Table 1 (*continued*)

		$x = 0.1$	$x = 0.2$	$x = 0.3$	$x = 0.4$
O6	Wyckoff		2m		
	x		0.3979(5)		
	y		0.2943(5)		
	U_{iso}($\times 100$ Å^2)		1.00(5)		
O7	Wyckoff		2m		
	x		0.7142(5)		
	y		0.4003(5)		
	U_{iso}($\times 100$ Å^2)		1.38(6)		
O_δ	Wyckoff	2e			
	U_{iso}($\times 100$ Å^2)	2.6(2)			
	S.O.F	0.373(6)			
R_p (%)	Bank 1	4.35	3.96	4.87	5.66
	Bank 3/5	4.74	5.68	4.71	6.40
R_{wp} (%)	Bank 1	6.10	5.20	6.64	7.34
	Bank 3/5	6.54	7.54	6.78	8.67
χ^2		3.800	1.446	2.461	1.361

[a] Isotropic displacement parameters of all Mn in the same structure were constrained to be equal to avoid unphysical values.
[b] O atom was refined displaced from the ideal 3d (0, 1/2, 0) position at 12 h one (see text).

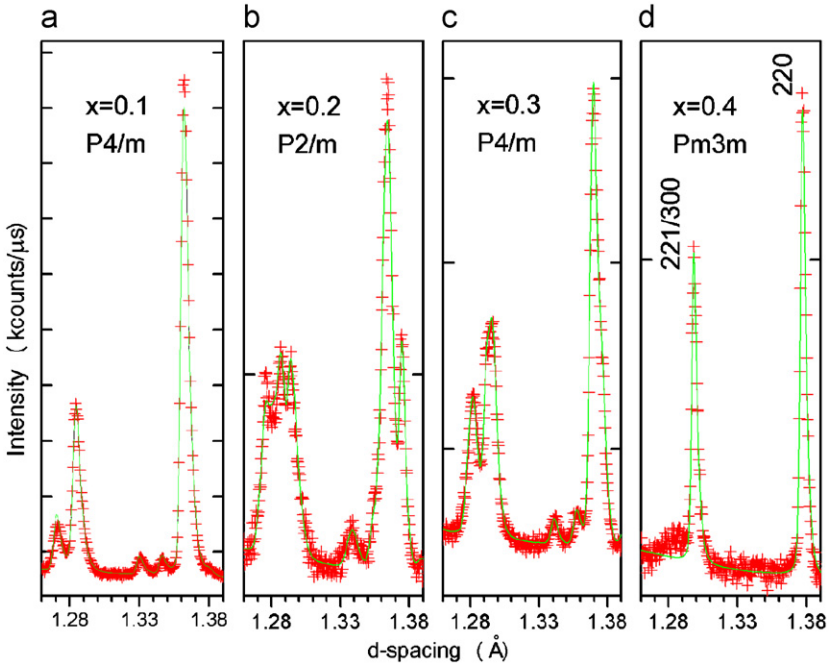

Fig. 3. Details of the neutron diffraction patterns near cubic 221/300 (left) and 220 (right) peaks highlighting splitting in the 1.26–1.39 Å d-spacing range for (a) tetragonal *P4/m* $(La_{0.1}Sr_{0.9})_5Mn_5O_{13.75}$, (b) monoclinic *P2/m* $(La_{0.2}Sr_{0.8})_5Mn_5O_{13}$, (c) tetragonal *P4/m* $(La_{0.3}Sr_{0.7})_5Mn_5O_{13}$ and (d) cubic *Pm3m* $La_{0.4}Sr_{0.6}MnO_{2.6}$. Normalization by one on the vertical axis represents 250 counts/μs. Colors and symbols are as in Fig. 2.

as $n = 4-5x$. This implies that the octahedral Mn^{4+} cation in $Sr_5Mn_5O_{13}$ $(x = 0)$ changes to $Mn^{3.5+}$ in $(La_{0.1}Sr_{0.9})_5Mn_5O_{13}$ $(x = 0.1$, in the absence of extra oxygen), to Mn^{3+} in $(La_{0.2}Sr_{0.8})_5Mn_5O_{13}$ $(x = 0.2)$, to $Mn^{2.5+}$ in $(La_{0.3}Sr_{0.7})_5Mn_5O_{13}$ $(x = 0.3)$ and to Mn^{2+} in a hypothetical long-range vacancy-ordered structure for $La_{0.4}Sr_{0.6}MnO_{2.6}$ $(x = 0.4)$. Charge reduction of the octahedral Mn1 site causes its significant size increase that has to be accommodated within geometrical constraints imposed by the constant geometry of Mn^{3+} pyramids. Apical Mn1–O bond distance of the octahedral Mn site shows only a slight increase with increasing x from 1.905 Å $(x = 0)$ to 1.926 Å $(x = 0.3)$ (see Table 2). The fixed size of the pyramids in the $x = 0$–0.3 compounds imposes constraints on Mn1–O1 bond distance. The charges of the octahedral Mn as derived from the Mn–O bond distances and bond valence sum (BVS) parameters (calculated using the program VALENCE [22]) are shown in Table 2. The Mn^{4+} cation

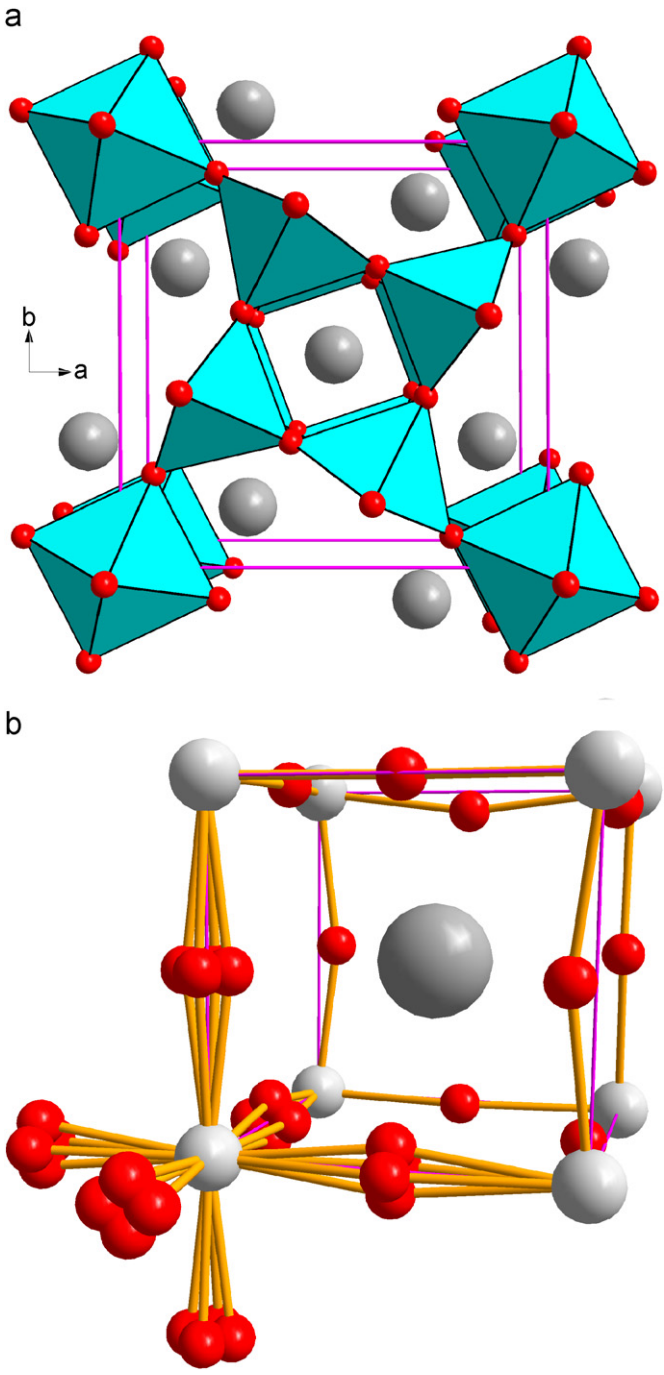

Fig. 4. Structure of (a) monoclinic $P2/m$ $(La_{0.2}Sr_{0.8})_5Mn_5O_{13}$ and (b) cubic $Pm3m$ $La_{0.4}Sr_{0.6}MnO_{2.6}$ obtained from Rietveld fits of neutron diffraction data. La^{3+}/Sr^{2+} cations and O^{2-} anions are represented as big dark-grey and small red spheres, respectively. All symmetry permitted positions for O^{2-} anions around Mn atom are shown for $La_{0.4}Sr_{0.6}MnO_{2.6}$ to emphasize the positional disorder described in text.

in $Sr_5Mn_5O_{13}$, with d^3 electronic configuration, shows almost undistorted octahedral coordination [3] as expected for three d electrons occupying the lower energy t_{2g} orbitals while both e_g orbitals pointing towards the O atoms are empty. The octahedral coordinated d^4 Mn^{3+} cation in $(La_{0.2}Sr_{0.8})_5Mn_5O_{13}$ has an additional electron that could either occupy one of the half-filled t_{2g} orbitals to give low-spin Mn^{3+} or occupy one of the empty e_g orbitals to give a high-spin electronic configuration. Trivalent Mn in low-spin state, to the best of our knowledge not observed in perovskite oxides to date, should produce shorter average Mn–O bonds than the high-spin, resulting in larger BVS values. This is not the case as the BVS values shown in Table 2 are identical for both octahedral and pyramidal Mn^{3+}. Since Mn in pyramids is high-spin [3,10,21], the octahedral Mn^{3+} appears to also assume high-spin electronic configuration. Therefore, the extra electron should be placed in one of the empty e_g orbitals and the octahedra should show Jahn-Teller distortion to reduce the energy of the otherwise degenerate half-occupied e_g levels.

The observed Mn^{3+}–O bond distances are atypical, however, for a high-spin state normally observed for Mn^{3+}. Four long (2×2.012 and 2×2.078 Å) and two short (2×1.912 Å) Mn–O bonds define a compressed MnO_6 octahedron.

Two possible explanations can be proposed for this finding that we will describe in the following. One possibility is that the observed bond distances appear as a consequence of the occupation of the $d_{x^2-y^2}$ orbital instead of the usually occupied d_{z^2} that would be empty in this case. The electronic configuration of Mn^{3+} in $(La_{0.2}Sr_{0.8})_5Mn_5O_{13}$ would then be $d^3_{t_{2g}}d^1_{x^2-y^2}d^0_{z^2}$ for the octahedra in contrast to the pyramids which show $d^3_{t_{2g}}d^0_{x^2-y^2}d^1_{z^2}$ configuration. Fig. 6a shows the proposed electronic configuration and octahedral distortion derived from it. A similar compressed Mn^{3+} octahedron has been proposed for the $La_{1.2}Sr_{0.8}MnO_{4.27}$ [23] compound using conventional X-rays. However, a disordered apical position was found in that compound, which could imply that the actual Mn–O apical bond distances extracted from the Rietveld refinement are reduced with respect to the real ones by the averaging of several oxygen atom positions. The apically compressed octahedral coordination of Mn^{3+} in $(La_{0.2}Sr_{0.8})_5Mn_5O_{13}$ with electronic configuration $d^3_{t_{2g}}d^1_{x^2-y^2}d^0_{z^2}$ would be, to the best of our knowledge, the first experimental observation of such a state for transition metal perovskites [24]. The second explanation could be that the observed bond distances do not originate form a single arrangement of oxygen around the octahedral Mn^{3+} but from the superposition of two different orientations of a typical elongated MnO_6 octahedra as is observed in $LaMnO_3$ [25] with the long and intermediate Mn–O bonds (2.178 and 1.968 Å, respectively) oriented in either x or y direction in the x–y plane and the short one (1.907 Å) always in the z direction. In such a case, both kinds of octahedral Mn^{3+} in $(La_{0.2}Sr_{0.8})_5Mn_5O_{13}$ would show a $d^3_{t_{2g}}d^0_{x^2-y^2}d^1_{z^2}$ electronic configuration and averaging of short and long Mn–O bonds in the x–y plane would explain the observed bond distances. Fig. 6b shows how, by overlapping two elongated octahedra rotated 90° with respect to each other in the x–y plane, the average compressed octahedra could be obtained with Mn–O bond distances approximately equal to those observed in $(La_{0.2}Sr_{0.8})_5Mn_5O_{13}$. Such elongated octahedra oriented in-plane would frustrate orbital arrangement and the bond lengths of two out of four adjacent pyramids. This may be a reason for a presence of two different pyramids in the refined $x = 0.2$ structure. However, since the long axis of JT-octahedron cannot be placed along the c-axis due to the size mismatch, this frustration may be also a good reason for the electron to occupy the x^2–y^2 orbital, which fits perfectly in-plane with an empty and short z^2 orbital along c-axis as proposed in first scenario. More high-resolution NPD data, structural local probes, as well as theoretical input are necessary to clarify this issue.

The second scenario is consistent with the breaking of the four-fold symmetry producing a monoclinic unit cell. The presence of disordered elongated octahedra lying in the x–y plane would break the local tetragonal symmetry of the system. On the contrary, if Mn^{3+} showed $d^3_{t_{2g}}d^1_{x^2-y^2}d^0_{z^2}$ electronic configuration, there would be no a-priori need to break it as the Mn^{3+} cation would still have an electronic configuration compatible with the 4-fold symmetry of the site. Moreover, the presence of disorder is consistent with the observation of small and anisotropic scattering domains that produce broadening of superstructure peaks. Finally, the observation of slightly different values of the

Table 2
Selected bond distances (Å) bond valence sums and average observed Mn valence for $La_xSr_{1-x}MnO_{2.6+\delta}$ ($x = 0$–0.4) compounds..

	$x = 0$ [3]	$x = 0.1$	$x = 0.2$		$x = 0.3$	$x = 0.4$
Octahedral						
Mn1–O_{ap}	1.9051(1) × 2	1.92042(2) × 2	1.91162(2) × 2		1.92606(3) × 2	1.9603 × 5.2
Mn1–O_{eq}	1.930(4) × 4	1.939(3) × 4	2.012(4) × 2		2.057(4) × 4	
Mn1–O_{eq}			2.078(4) × 2			
BVS	3.8 (Mn^{4+})	3.7 (Mn^{4+})	3.2 (Mn^{3+})		3.06 (Mn^{3+})	2.9 (Mn^{3+})[a]
Pyramidal			Mn2	Mn3		
Mn2/3–O_{ap}	2.058(4)	1.987(4)	1.968(8)	2.082(8)	1.987(5)	
Mn2/3–O_{eq}	1.9212(5) × 2	1.9272(3) × 2	1.9397(12) × 2	1.9213(7) × 2	1.9374(6) × 2	
Mn2/3–O_{eq}	1.938(5)	1.942(4)	1.906(7)	1.932(7)	1.934(7)	
Mn2/3–O_{eq}	1.846(4)	1.874(4)	1.869(8)	1.863(7)	1.862(7)	
Mn2–O_{δ}		1.906(3)				
BVS	3.2 (Mn^{3+})	3.2(3+)/3.8(4+)	3.2 (Mn^{3+})	3.1 (Mn^{3+})	3.2 (Mn^{3+})	
Avg. Mn valence	3.20+	3.38+	3.00+		2.90+	2.80+

[a] Coordination index 5 was assumed for this calculation.

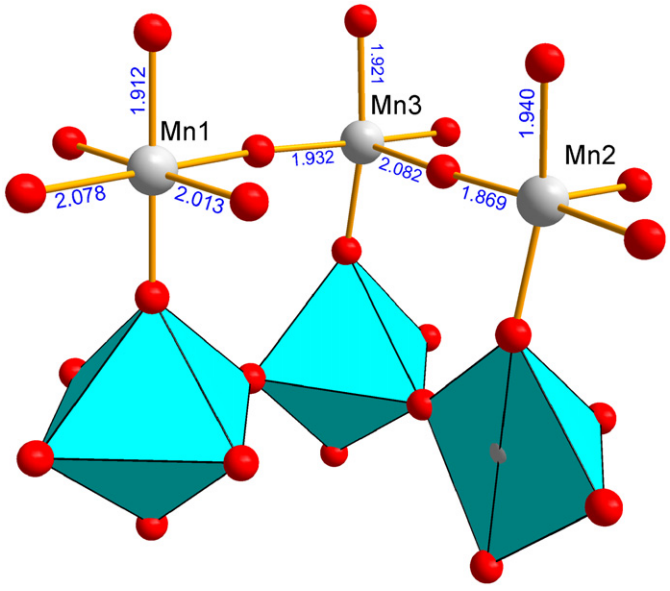

Fig. 5. Coordination polyhedra around Mn atoms for $(La_{0.2}Sr_{0.8})_5Mn_5O_{13}$. Color scheme is as in Fig. 4. Relevant bond distances are given (Å).

monoclinic angle with different thermal treatments of the sample could also be explained by the fact that different degrees of disorder of the elongated octahedra would produce slightly different average structures.

In a previous report based on lower resolution data [4], we have modeled the structure of $(La_{0.2}Sr_{0.8})_5Mn_5O_{13}$ between 500 and 700 °C using a tetragonal $P4_2/m$ space group where ordering of elongated octahedra alternating along between the x and y directions is possible. Such a model gave a poor fit to the higher resolution room temperature data, confirming the absence of long-range ordering in the direction of the apical elongation of Mn^{3+} octahedra in the x–y plane.

Similar compressed Mn–O octahedral coordination is observed for the $x = 0.3$ compound $(La_{0.3}Sr_{0.7})_5Mn_5O_{13}$ where 50% of the Mn1 site is occupied by d^5 Mn^{2+} cations. Since the Mn1 site is, on average, even larger than in $(La_{0.2}Sr_{0.8})_5Mn_5O_{13}$ we still assign a high-spin electronic configuration to both Mn^{2+} and Mn^{3+} cations (low-spin configuration of $Mn^{2+}$is even less favored than for Mn^{3+} due to the large exchange energy loss). The BVS for Mn1 cation using Mn^{3+} parameters for the calculation supports this picture; BVS decreases from 3.2 in $x = 0.2$ to 3.06 in $x = 0.3$ indicating reduction of the average charge of Mn1 site with x. The non-Jahn-Teller high-spin Mn^{2+}–O bond lengths (with both e_g orbitals half-filled) do not conform to the required short Mn1–O distance. Average Mn^{2+}–O bond distances for $(La_{0.3}Sr_{0.7})_5Mn_5O_{13}$ are at least 0.1 Å longer than the average bond observed in $(La_{0.2}Sr_{0.8})_5Mn_5O_{13}$, therefore huge chemical pressure, alleviated only by the presence of disordered Mn^{3+} and Mn^{2+} octahedra, is present in this compound as extracted from the high value of the calculated BVS for the Mn1 site. The diffraction data still shows significant superstructure-peaks broadening but an overall tetragonal symmetry is observed. No indication for the presence of superstructures arising from coherent orientations of the Mn^{3+} octahedra has been found in the analyzed data.

The concentration of Mn^{3+} elongated octahedra may explain the change in symmetry from P4/m for $x = 0.1$ to P2/m ($x = 0.2$) and back to P4/m for $x = 0.3$. For both $x = 0.1$ and 0.3 the Mn^{3+} coexist with an equal number of isotropic Mn^{4+} or Mn^{2+} cations, respectively. These cations form regular octahedra conforming to the 4/m symmetry, therefore, the local distortion caused by the Mn^{3+} anisotropic octahedron is diluted in the network. For $x = 0.2$, only the elongated Mn^{3+} octahedra with the long axis lying in the x–y plane in a disordered manner are present. The relative orientation of these octahedra in different structural domains does not perfectly average into a tetragonal structure; i.e., the 2/m symmetry of the octahedral sites persists in the average structure with the degree of distortion depending on the sample preparation conditions.

The oxygen-vacancy ordering and orbital ordering of Mn^{3+} pyramids is finally destabilized with respect to the formation of an oxygen-vacancy disordered cubic phase in $La_{0.4}Sr_{0.6}MnO_{2.6}$ for which only Mn^{2+} would be found in hypothetical long-range oxygen-vacancy-ordered $(La_{0.4}Sr_{0.6})_5Mn_5O_{13}$ compound. This vacancy-disordered phase shows, however, clear signs of local ordering in domains smaller than the neutron sampling volume as confirmed by the observation of displacement of O anions from the ideal crystallographic position for the cubic perovskite phase and the increased background in regions of the diffraction patterns where superstructure peaks are present for the other compounds, as discussed before.

4. Conclusions

The oxygen-vacancy-ordered phases $(La_xSr_{1-x})_5Mn_5O_{13}$ ($x = 0.1$–0.3) and vacancy-disordered $La_{0.4}Sr_{0.6}MnO_{2.6}$ have

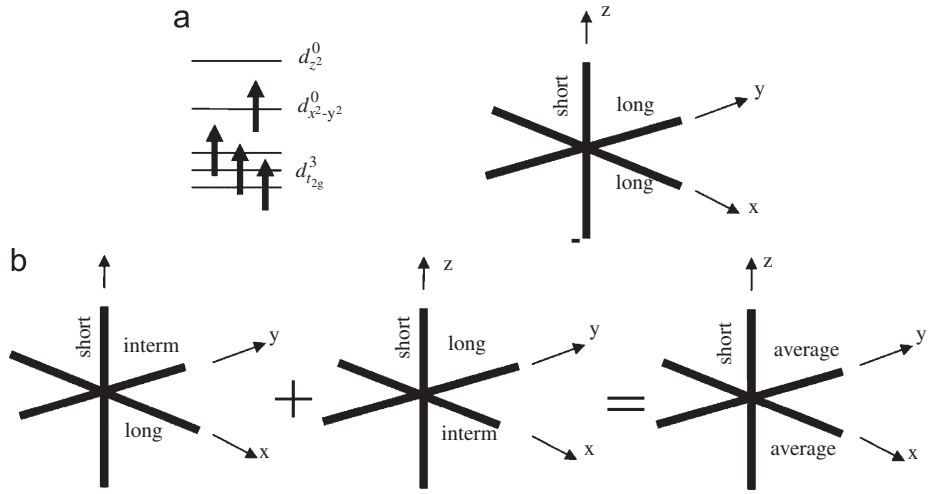

Fig. 6. Two possible explanations for the observed Mn–O bonds in the octahedral Mn^{3+} cation in $(La_{0.2}Sr_{0.8})_5Mn_5O_{13}$: (a) the electronic configuration of the d^4 Mn^{3+} cation is $d^3_{t_{2g}}d^1_{x^2-y^2}d^0_{z^2}$ making O atoms in the plane move further away from the cation while the apical Mn–O bond is unchanged respect to $x=0$ and 0.1 compounds; (b) the observed octahedron is the averaging of two apically elongated Mn^{3+} octahedra with the long and intermediate bonds in the x–y plane and a short one in the z direction.

been prepared and their structures characterized by neutron time-of-flight powder diffraction. The vacancy-ordered phases show common structural features with the previously studied compound $Sr_5Mn_5O_{13}$ ($x=0$), that contains in its structure four orbital-ordered Mn^{3+} pyramids and one octahedral Mn cation that changes its charge from Mn^{4+} in $x=0$ through Mn^{3+} in $x=0.2$ to $Mn^{2.5+}$ in $x=0.3$. The change from non-Jahn-Teller Mn^{4+} to Jahn-Teller Mn^{3+} requires distortions of the octahedral coordination constrained by the fixed geometry of the Mn^{3+} pyramids in the z direction that results in observation of compressed Mn^{3+} octahedra. This geometry can be interpreted in two ways: (1) the electronic configuration of Mn in the octahedral site is a novel $d^3_{t_{2g}}d^1_{x^2-y^2}d^0_{z^2}$ as compared to the typical $d^3_{t_{2g}}d^0_{x^2-y^2}d^1_{z^2}$ for Mn^{3+} in pyramidal sites or (2) the disordered Mn^{3+} apically elongated octahedra are present with normal electronic configuration $d^3_{t_{2g}}d^0_{x^2-y^2}d^1_{z^2}$, and the observed bond distances are the average of the long and intermediate in-plane Mn–O bonds typical for the elongated MnO_6 octahedra. Several structural features favor the second case, however, further high-resolution diffraction and local probes should be used to unambiguously confirm that. The decrease in charge and increase in size of the octahedral Mn site produced by La substitution finally destabilizes the vacancy-ordered structure producing a vacancy-disorder phase for $x=0.4$ that shows clear signs of short-range vacancy ordering through the displacement of oxygen atoms from the ideal site in the cubic perovskite structure.

Acknowledgements

This work was carried out during LS's stay at Argonne National Laboratory. Work at NIU was supported by the NSF-DMR-0706610 and by the US Department of Transportation. Work at Argonne's IPNS was supported by the US Department of Energy, Office of Science, Office of Basic Energy Sciences, under Contract DE-AC02-06CH11357.

References

[1] R.H. Mitchell, Perovskites: Modern and Ancient, Almaz Press Inc., Thunder Bay, 2002.
[2] T. Mori, N.J. Kamegashira, J. Alloys Compd. 408–412 (2006) 1210–1213.
[3] L. Suescun, O. Chmaissem, J. Mais, B. Dabrowski, J.D. Jorgensen, J. Solid State Chem. 180 (2007) 1698–1707.
[4] L. Suescun, B. Dabrowski, J. Mais, S. Remsen, J.W. Richardson Jr., E.R. Maxey, J.D. Jorgensen, Chem. Mater. 20 (2008) 1636–1645.
[5] B. Dabrowski, J.E. Greedan, M. Greenblat, C.P. Grey, A.J. Jacobson, D.A. Keszleer, J. Li, M.A. Subramanian, Y. Xia, in: M.G. Kanatzidis, K.R. Poeppelmeier (Ed.), Prog. Solid State Chem., vol. 36, 2007, pp. 1–133.
[6] L.J. Gauckler, D. Beckel, B.E. Buergler, E. Jud, U.R. Muecke, M. Prestat, J.L.M. Rupp, J. Richter, Chimia 58 (2004) 837–850.
[7] M.L. Ruiz-González, R. Cortés-Gil, J.M. Alonso, A. Hernando, M. Vallet-Regí, J.M. González-Calbet, Chem. Mater. 18 (2006) 5756–5763.
[8] P.S. Casey, D. Barker, M.A. Hayward, J. Solid State Chem. 179 (2006) 1375–1382.
[9] P.K. Gallagher, J.B. MacChesney, D.N.E. Buchanan, J. Chem. Phys. 41 (1964) 2429–2434.
[10] K.R. Poeppelmeier, M.E. Leonowicz, J.C. Scanlon, J.M. Longo, W.B. Yelon, J. Solid State Chem. 45 (1982) 71–79.
[11] L. Suescun, B. Dabrowski, Acta Crystallogr. Sect. B: Struct. Sci. 64 (2008) 177–186.
[12] B. Dabrowski, O. Chmaissem, J. Mais, S. Kolesnik, J.D. Jorgensen, S. Short, J. Solid State Chem. 170 (2003) 154–164.
[13] O. Chmaissem, B. Dabrowski, S. Kolesnik, J. Mais, J.D. Jorgensen, S. Short, Phys. Rev. B 67 (2003) 94431.
[14] J.D. Jorgensen, J.M. Carpenter, R.K. Crawford, J.R. Haumann, R.L. Hitterman, R. Kleb, G.E. Ostrowski, F.J. Rotella, T.G. Worlton, J. Appl. Crystallogr. 22 (1989) 321–333.
[15] A.C. Larson, R.B. Von Dreele, General Structure Analysis System (GSAS); Los Alamos National Laboratory Report LAUR 86-748; Los Alamos National Laboratory: Los Alamos, NM, 2004.
[16] B.H. Toby, J. Appl. Crystallogr. 34 (2001) 210–221.
[17] P.W. Stephens, J. Appl. Crystallogr. 32 (1999) 281–289.
[18] C. Michel, L. Er-Rakho, B. Raveau, Mater. Res. Bull. 20 (1985) 667–671.
[19] S.J. La Placa, J.F. Bringley, B.A. Scott, D.E. Cox, J. Solid State Chem. 118 (1995) 170–175.
[20] B.-H. Chen, D. Walker, E. Suard, B.A. Scott, B. Mercey, M. Hervieu, B. Raveau, Inorg. Chem. 34 (1995) 2077–2083.
[21] V. Caignaert, J. Magn. Magn. Mater. 166 (2000) 117–123.
[22] I.D. Brown, J. Appl. Crystallogr. 29 (1996) 479–480.
[23] R.K. Li, C. Greaves, J. Solid State Chem. 153 (2000) 34–40.
[24] D. Khomskii, J. van den Brink, Phys. Rev. Lett. 85 (2000) 3329.
[25] J. Rodriguez-Carvajal, M. Hennion, F. Moussa, A.H. Moudden, Phys. Rev. B 57 (1998) R3189–R3192.